



1

2 **Study of Magnetosphere Dynamics under Various Alfven Mach Numbers for the**
3 **Northward IMF Condition: 3D Global PIC Simulations**

4 Amin Esmaeili^{1,*}, Muhammad Ikram², Abdullah Khan³, Abid Ali Abid³

5 ¹University of Tehran, Institute of Geophysics, Space Physics group, Tehran, Iran

6 ² Department of Physics, Hazara University, 21300 Mansehra, Pakistan

7 ³CAS Key Laboratory of Geospace Environment, Department of Geospace and Planetary
8 Science, University of Science and Technology of China, Hefei, Anhui 230026, China

9 *Corresponding author, email:amin.esmaeili@gmail.com

10 **Abstract**

11 For a long time, the interactions of the solar wind with the Earth's magnetosphere
12 have been analyzed with the help of three-dimensional (3D) global particle-in-cell (PIC)
13 simulation where the interplanetary magnetic field (IMF) is steadily northward. Yet the
14 Earth's magnetosphere and the Kelvin-Helmholtz Instability (KHI) in a global, dayside
15 and nightside magnetotail configuration using the 3D PIC simulations has not been well
16 examined. In this work, we compared the simulation results for both high and low Alfven
17 Mach numbers of $MA=5$ and $MA=1$, respectively. Our results show diverse
18 magnetospheric dynamics by taking into account the various Alfvenic Mach conditions.
19 The relationship between the upstream magnetohydrodynamic (MHD) turbulence in the
20 solar wind and Earth's magnetosphere behavior is investigated. In both the meridian and
21 equatorial planes, the effects of Alfven Mach number on magnetospheric characteristics
22 such as electron/ion densities and current densities are explored. The structure of the
23 magnetosphere is also investigated at high and low Alfven Mach numbers. The solar-
24 terrestrial interaction as a result of various solar activities is investigated in this work
25 utilizing a large-scale global three-dimensional PIC simulation.



Keywords: Northward IMF, Kelvin-Helmholtz Instability, Magnetosphere dynamics, 3D
PIC simulation, Alfvén Mach number.

1- Introduction:

The interplanetary magnetic field (IMF) has long been believed to play a huge rule in the solar wind interactions with the Earth's magnetosphere. Beyond the Earth magnetosphere, particles entering the Earth's surface may have a wide range of impacts on our daily lives. The magnetic fields of the Sun are primarily triggered the activity of the solar cycle effects on the Sun's surface like sunspots. The amount of activity on the Sun's surface changes as the magnetic fields change. The Earth may be affected by this activity such as, the eruptions can cause lights in the Earth's magnetosphere called aurora. The radio communications and even the electricity grids on Earth may be affected by the extreme eruptions and avalanches of high-energy particles reaching the Earth's surface during the high solar activity. Aerosols are the primary constituents of clouds and are formed by energetic particles trapped by the Earth's magnetosphere. Bow shock is formed on the dayside at (11-14) R_E when the solar wind strike against the Earth's magnetosphere, where R_E is the Earth radius. Lugaz et al. [2016] studied that a bow shock will occur when the solar wind's magnetosonic Mach number is larger than one. The Earth's magnetosphere encompasses different regions, for instance, the radiation belts, Van Allen bands, plasmasphere, and ionosphere. However, all these magnetosphere's boundaries would be affected by the solar wind's magnetic field, dynamic pressure, and number density, which are all associated to the Alfvén Mach number. Several Mach regimes have been used to study the interaction of the solar with the Earth (Farrugia et al. 1995; Lavraud



49 & Borovsky 2008). Most prior investigations have been concluded that the
50 magnetopause location is determined by the solar wind's dynamic pressure. Fairfield
51 (1971) and Shue et al. found the influence of the IMF orientation on the location of
52 the magnetopause.

53 In this paper, the 3D PIC simulation has been performed to investigate the effect
54 of different Alfvén Mach numbers ($MA=1$ and 5) on the general shape, size,
55 ion/electron concentrations, currents, and overall dynamics of the magnetosphere.
56 We also compared the findings of the 3D PIC simulation to the results of the MHD
57 simulation (Lavraud & Borovsky 2008).

582. Simulation Model

59 The basic MHD equations are as follows.

$$60 \quad \frac{\partial B}{\partial t} = -c \nabla \times E \quad (1)$$

$$61 \quad \frac{\partial E}{\partial t} = c^2 \nabla \times B - \frac{1}{\epsilon_0} J \quad (2)$$

$$62 \quad m_{i,e} \frac{dv_{i,e}}{dt} + q_{i,e} (E + v_{i,e} \times B) \quad (3)$$

63 where B represents the magnetic field, E is the electric field, J is the current
64 density and v is the charged particle velocity. Furthermore, c is the speed of light,
65 q is the particle charge, and m is the particle mass while the subscripts i and
66 e stand for ions and electrons, respectively.

672-1 Initial parameters:



68 In this paper, the typical values of the Mach numbers, $MA=1$ and $MA=5$ are used to
69 examine the Earth's magnetospheric dynamics. Alfvén Mach number is the ratio of the
70 bulk velocity to the Alfvén velocity $MA = V_{Bulk} / V_{Alfvén}$ where $V_{Alfvén} = B / \sqrt{\mu_o \rho}$ with
71 B is the magnetic field (here B is considered as IMF magnetic field), μ_o is the
72 vacuum permeability and ρ is the charge density. For this simulation, we used the
73 latest version of the 3D Stanford PIC code (Tristan code) (Buneman et al. 1992;
74 Buneman 1993; Cai et al. 2015). A 3D electromagnetic complete particle global
75 simulation model is also used in this study. This simulation model divides the temporal
76 sequence of IMF rotations into two phases (i) the Earth's magnetosphere is produced by a
77 magnetic dipole field from time step 0 to 1500, during which there is no IMF (ii) a
78 northward IMF ($B_z=0.215$) gradually activates from the step 1501 to 1800. The IMF then
79 remains unchanged until the time step reaches to 3000 (Esmaili & Kalaei 2017).

80 In this paper, we adopt the same simulation model with dimensions ($x=215$,
81 $y=145$, $z=145$) that has previously been used by Esmaili & Kalaei [2017] and Esmaili
82 et al. [2020]. In the simulation, 1 equals to $0.5 R_E$ where $1 R_E$ is approximately
83 6400 km. The 1000 simulation time step would be roughly 26 minutes if we take a
84 typical value of 400 km/s for solar wind velocity and each grid spacing (Need to be
85 rephrased). In this work, a magnetic field is normalized to the reference magnetic field
86 which is equal to, in which is the electron mass and is the electron plasma frequency and
87 e is the electron charge.



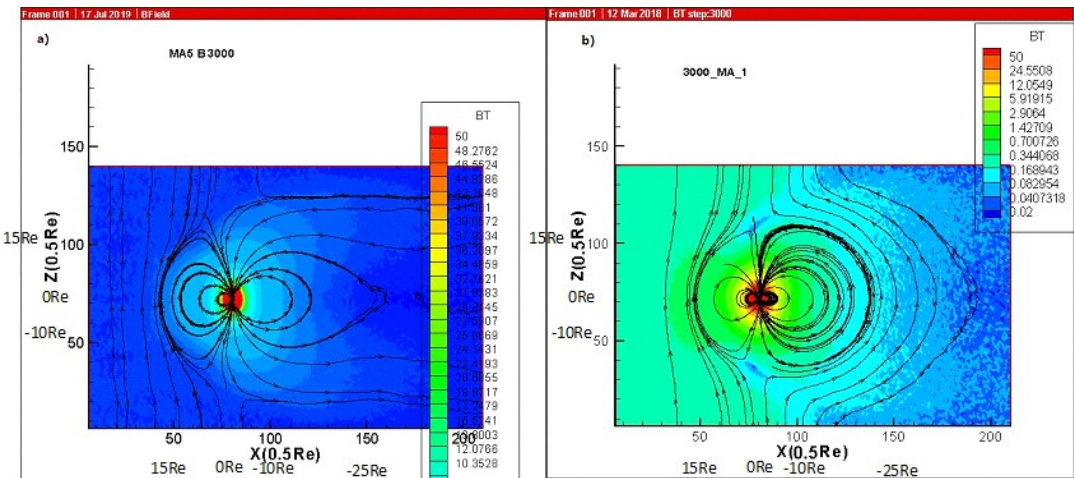
88 Alfvén Mach number is the ratio of the bulk velocity to the Alfvén velocity (v_{A}). Alfvén
89 velocity is defined as $v_{\text{A}} = B / \sqrt{\mu_0 \rho}$, whereas B is the magnetic field (here is the magnetic field of IMF)
90 and μ_0 is the vacuum permeability and ρ is the density. For this simulation, we used the latest
91 version of the 3D Stanford PIC code (Tristan code) (Buneman et al. 1992; Buneman
92 1993; Cai et al. 2015).

93 **2 MA effects on the general shape of magnetosphere during northward IMF**

94 direction in the meridian plane (Section Name is Confusing):

95 **2 Effect of MA on the Structure of Earth's Magnetosphere**

96 The solar-terrestrial total magnetic field during the northward IMF direction is depicted
97 in Figure 1. The near-Earth cusp axis is perpendicular to the magnetopause of the
98 magnetospheric flanks as shown in Figure 1. The cusp axis is tilted sunward using the
99 typical value of $MA(=5)$. In this case, the reconnection zone region is relocated to the
100 lower latitude, almost above the cross-section of the cusp axis with the magnetopause.



101
102 Fig.1 General magnetospheric shapes in the meridian plane, during northward IMF
103 condition for (a) $MA=5$, (b) $MA=1$ (compared to figure 3, Lavraud & Borovsky 2008),
104 Black lines in a) and b) represent the cusp axis.

105



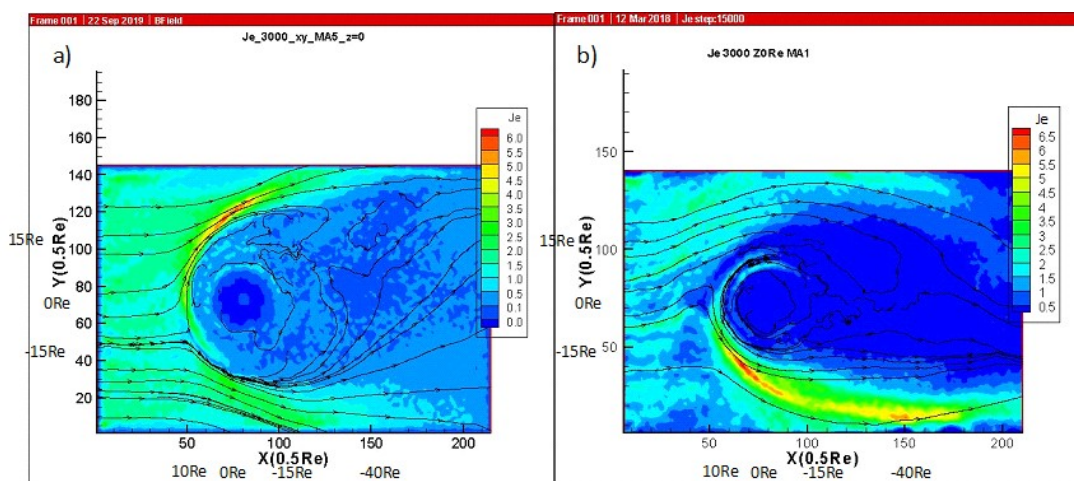
106 This is in good agreement with MHD simulation results by Lavraud & Borovsky (2008).
107 In addition, a more compact magnetosphere configuration is produced using the typical
108 value of $MA(=1)$. However, we observed the closed magnetic field lines in the near-Earth
109 magnetotail about $X=180$ while the magnetosphere is opened in the tail ward using
110 $MA=5$ as depicted in Figure 1b. This agrees well with the ~~of the~~ MHD simulation results
111 (Lavraud & Borovsky 2008, Figure 3).

112 The Earth's magnetotail acts as a reservoir for the energy that is extracted from the
113 interaction between the solar wind and the Earth's magnetosphere. A portion of that
114 energy is released through a violent process known as a magnetospheric substorm.
115 Behind the Earth, the solar wind extends the magnetosphere away from the Earth on the
116 nightside forming the magnetotail. The magnetotail contains two lobes, such as northern
117 and southern tail lobes which are separated by a plasma sheet (it is an area where the
118 magnetic field is weaker). The magnetic field lines looks dipolar in the near-Earth
119 magnetotail ($MA=1$) while the field lines are stretched by increasing the value of $MA(=5)$
120 as shown in Figure 1. Furthermore, the thin current sheet region is formed by increasing
121 the MA value.

122 Next, we will compare the previous MHD simulation findings are on the equatorial plane
123 with our results which are obtained for the meridian plane. The resemblance of the MHD
124 simulation results with the current equatorial plane findings will be investigated in the
125 following sections.

126 2-3 Total electron/ion current density in the equatorial plane:

127 Figure 2 shows the total electron current densities in the equatorial plane both for
128 $MA=5$ and $MA=1$:

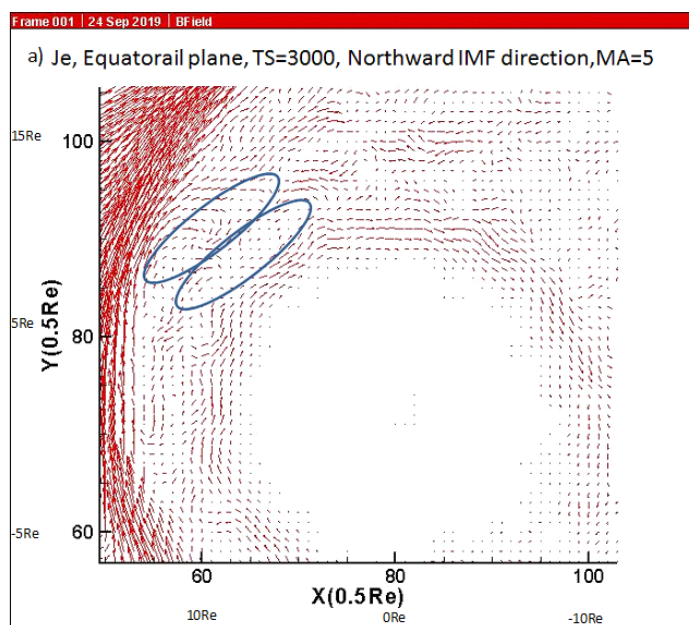


129

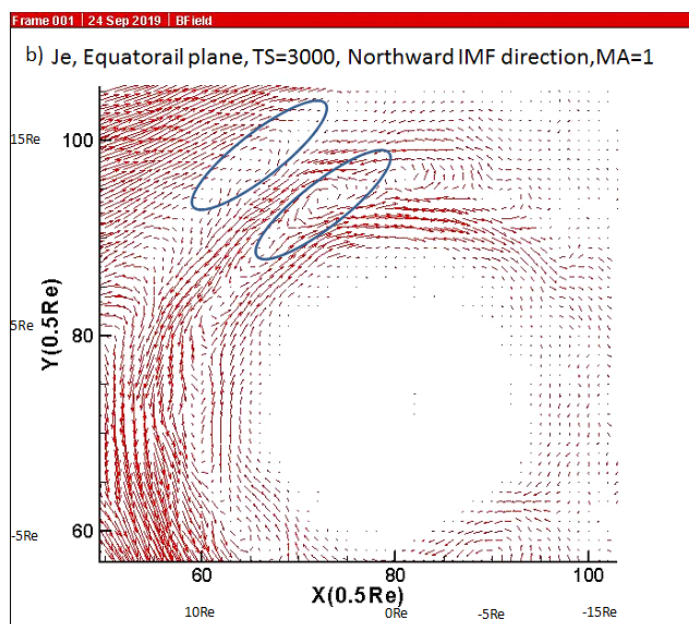
130 Fig. 2 Total electron current densities in the equatorial plane, during northward IMF
 131 condition for (a) MA=5, (b) MA=1

132

133 In the higher MA case, we can see more intense and turbulent currents around the Earth
 134 than in the lower MA counterpart. A ring current is the result of trapping the charged
 135 particles in a Earth's magnetosphere and this ring current is larger for MA=5 case (Fig.
 136 1a) (The figure cite here maybe wrong). For the case of MA=5, we observed a maximum
 137 current density area in the dusk-side of the Earth (about $Y=120$ in Fig 2a) and a similar
 138 area in the dawn-ward of the Earth (around $Y=50$ in Fig 2b) for the MA=1 case.



139



140

141 Fig.3 Total electron current density vectors in the equatorial plane, $Z=0\text{Re}$, during
 142 northward IMF condition for (a) $MA=5$, (b) $MA=1$

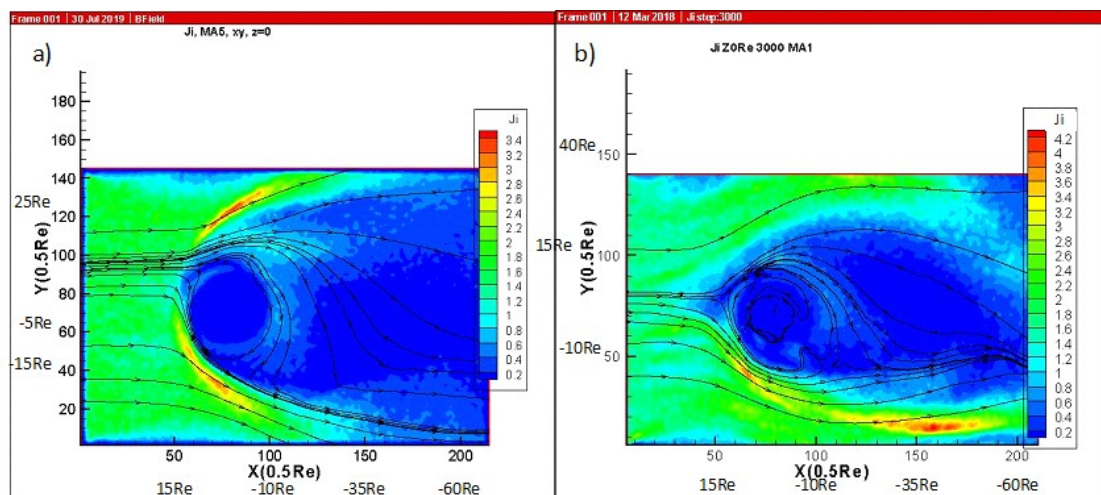
143



144The velocity shear on the magnetosphere's boundary layer can trigger the Kelvin-
 145Helmholtz Instability (KHI, vortexes in the ovals in Fig 3a, b) , which is important to
 146physicists because it could be the potential candidates for mass and energy transfer from
 147the solar wind to the magnetosphere. Using their three-dimensional MHD code, Merkin
 148and his colleagues (2013) evaluated the magnetopause's stability in terms of KHI growth
 149rate. The velocity shear between the magnetospheric plasma (which is essentially
 150stagnant) and the magnetosheath flow drives this growth rate (These sentences are
 151confusing). They discovered that magnetic tension is critical in the stabilization of
 152oscillation growth rates (One can't state the stabilization of the growth rates, this is
 153misleading) . Matsumoto & Seki (2007) used 3D MHD simulation to examine KHI
 154under various beta conditions, where beta is the ratio of plasma pressure to magnetic
 155pressure. They changed the beta parameter to investigate the effect of magnetic field
 156intensity on the KHI's 3D nonlinear evolution. They have found ~~discovered~~ that the
 157vortex shape is unstable at high beta and more stable at low beta. In addition, using a 2D
 158MHD code, Samtaney (2003) demonstrated the magnetic field's ability to inhibit
 159Ritchmaier-Meshkov instability (This sentence is confusing. I think, the work 2003
 160should be cited earlier than 2007). In terms of the more stabilised condition under lower
 161 $MA = 1$ case, our 3D PIC simulation results are in good agreement with the 3D MHD
 162simulation results obtained by Merkin et al. [2013]; Matsumoto & Seki [2007]; and
 163Samtaney [2003]. The vector plot of electron current density is shown in Figure 3. For
 164both $Ma=5$ and $Ma=1$, it seems similar to the to Figure 2. In the case of $MA=5$, there are
 165more turbulent currents around the plasmasphere (Figure 3a). However, for the lower



166Alfvén Mach number case, the two layers of Kelvin-Helmholtz instability (Ovals in the
 167plots) are more apparent.



168

169Fig.4 Total ion current densities in the equatorial plane, $Z=0$ Re, during northward IMF
 170condition for (a) $MA=5$, (b) $MA=1$

171The total ion current density in the equatorial plane for the two situations of Mach Alfvén
 172numbers is shown in Figure 4. For the situation of $MA=5$ in Fig.4a, we have a wider eye
 173structure of the ion current density in the equatorial plane. However, the eye shape is
 174twisted Sunward when $MA=1$ as depicted in Figure 4b. The Alfvén Mach number has a
 175significant influence on various dynamics as well as the topologies of the Earth's
 176magnetosphere, as shown in Figure 4.

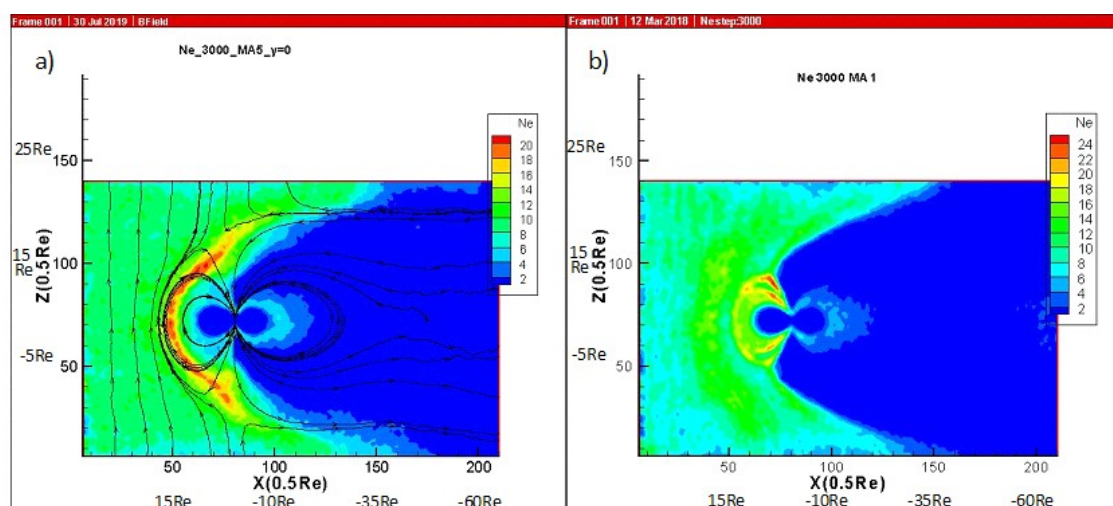
1772-4 Electron/ion number densities:

178Figure 5 illustrates the electron number densities for both Mach numbers of $MA=1$ and
 179 $MA=5$ in the meridian plane. In the case of $MA=5$, electrons accumulated in the cusp
 180area at higher altitudes, as well as near the magnetosheath, as seen in Fig. 5a. In addition,
 181in Fig. 5b, the double cusp structure can be seen for $MA=1$, but it is not visible for



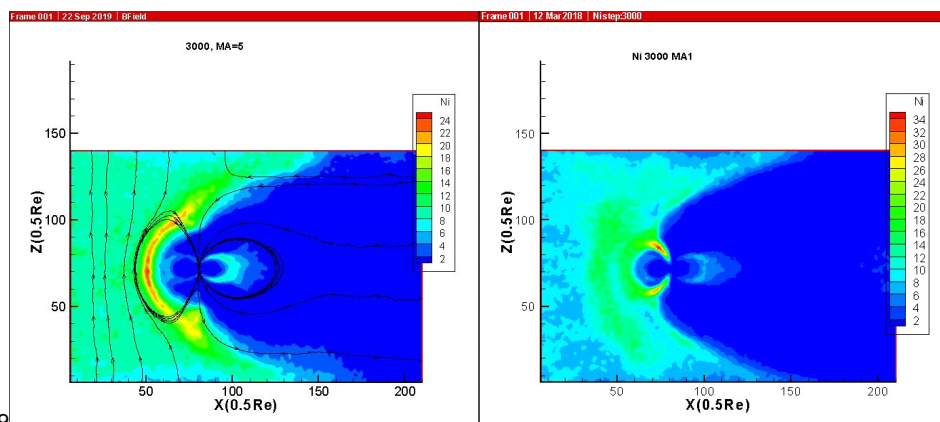
182MA=5. In addition, when the Mach number becomes larger, the magnetosheath structure
 183appears to be smaller.

184



185
 186Fig.5 Total electron number densities in the meridian plane during northward IMF
 187condition for (a) MA=5, (b) MA=1

188



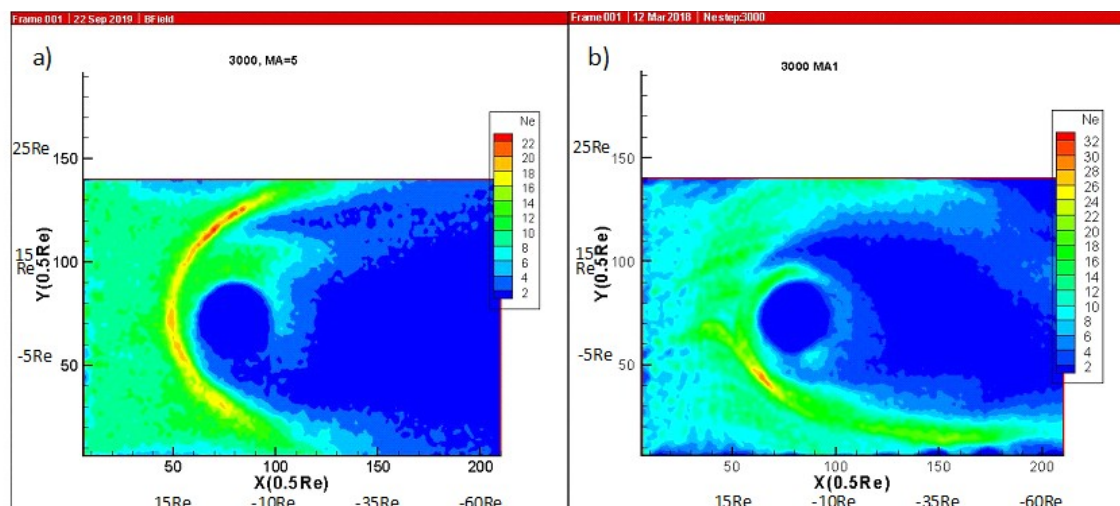
189
 190Fig.6 Total ion number densities in the meridian plane during northward IMF condition
 191for (a) MA=5, (b) MA=1

192



Ion number densities in the meridian plane for various Alfvén Mach numbers in the northward IMF direction are shown in Figure 6. The different field topologies of the magnetosphere alter with the ion distributions in the magnetosphere (Fig. 6a, b). Ions appear to be accumulating in the magnetosheath mostly around the Sun–Earth line with $MA=5$ rather than its lower counterpart.

198



199
 200 Fig. 7 Total electron number densities in the equatorial plane during northward IMF
 201 condition for (a) $MA=5$, (b) $MA=1$

202

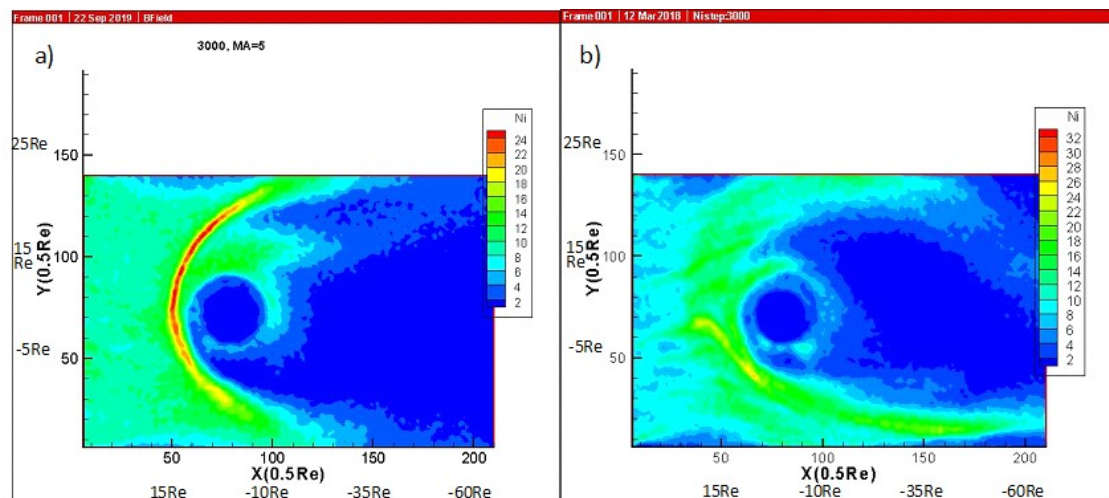
203

The electron densities in the equatorial plane are shown in Figure 7 for both high and low Alfvén Mach numbers. In the event of a higher MA , we can witness more electrons accumulating near the Earth than in the case of a lower Alfvén Mach number. From the dawn to the dusk ward of the Earth, increasing density of electrons may be seen in Fig. 7a. Only in the dawn-ward region of the Earth does Fig 7b exhibit high quantities of



209electrons. Furthermore, the maximum number density areas in both MA=5, 1 match to
 210the maximum current areas in Figures 2-a, b.

211



212
 213Fig.8Total ion number densities in the equatorial plane during northward IMF condition
 214for (a) MA=5, (b) MA=1

215

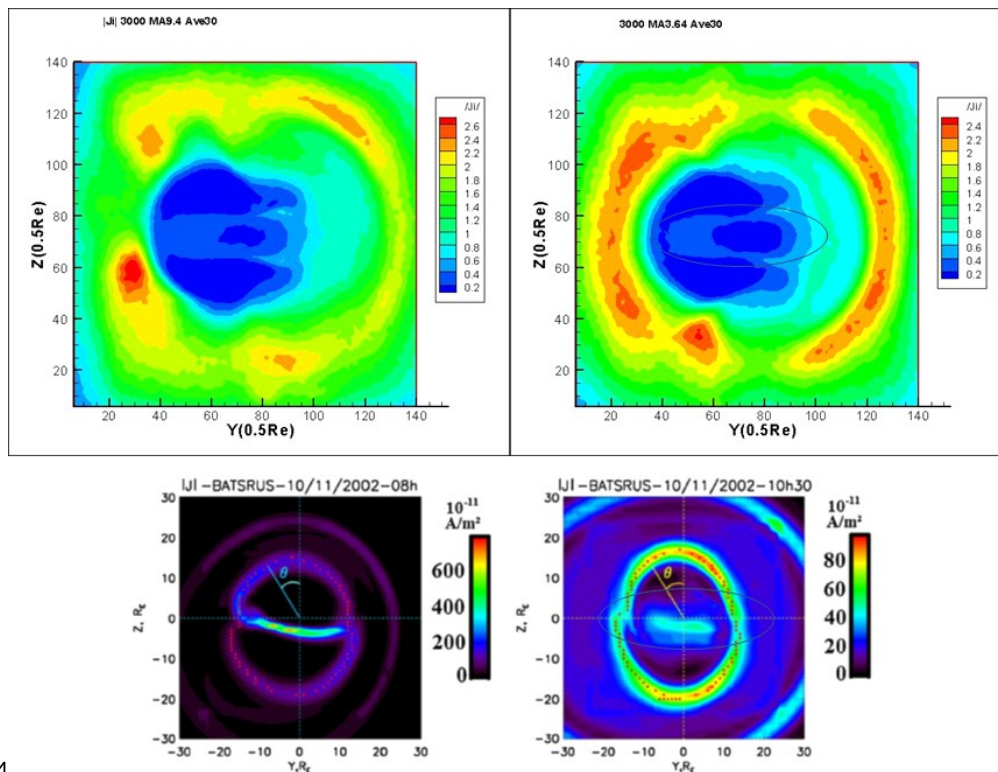
216In the equatorial plane, the maximum ion density can be seen in the dusk-side of the
 217Earth for MA=5 in figure 8a, compared to the dawn-side of the Earth for MA=1 in figure
 218b. The electron and ion densities have nearly identical behavior as the values of Mach
 219number increases.

2204-Simulation benchmarks

221 The current results using the 3D global PIC simulations has an extensive benchmark
 222with the experimental results from the CLUSTER satellite and also benchmark with the
 223previous 3D MHD findings obtained by Cai et al [2015]. Also, for the case shown in
 224figure 1, we have showed the good agreement with the previous MHD results (e.g. see
 225figure 3, in Lavraud 2008) for the general shape of magnetosphere due to the different



226MA numbers. Also, cusp axis sunward tilt in Figure 1b using MA=5 is in a good
 227agreement with MHD results (e.g. see Lavraud & Borovsky 2008). Higher values of the
 228Alfven Mach number shift magnetic reconnection to a lower altitude, which is consistent
 229with previous MHD simulation findings by Lavraud & Borovsky [2008]. The less
 230turbulent vortices of Kelvin Helmholtz instability inside the Earth's magnetosphere using
 231MA=1 in Fig 3b has also good agreement with the MHD results from by Merkin et al
 232[2013], Matsumoto & Seki [2007] and Samtaney [2003]. Figure 9 shows the PIC
 233simulation results and MHD results in the lower row for both MA =3.64 and MA=9.4:



234

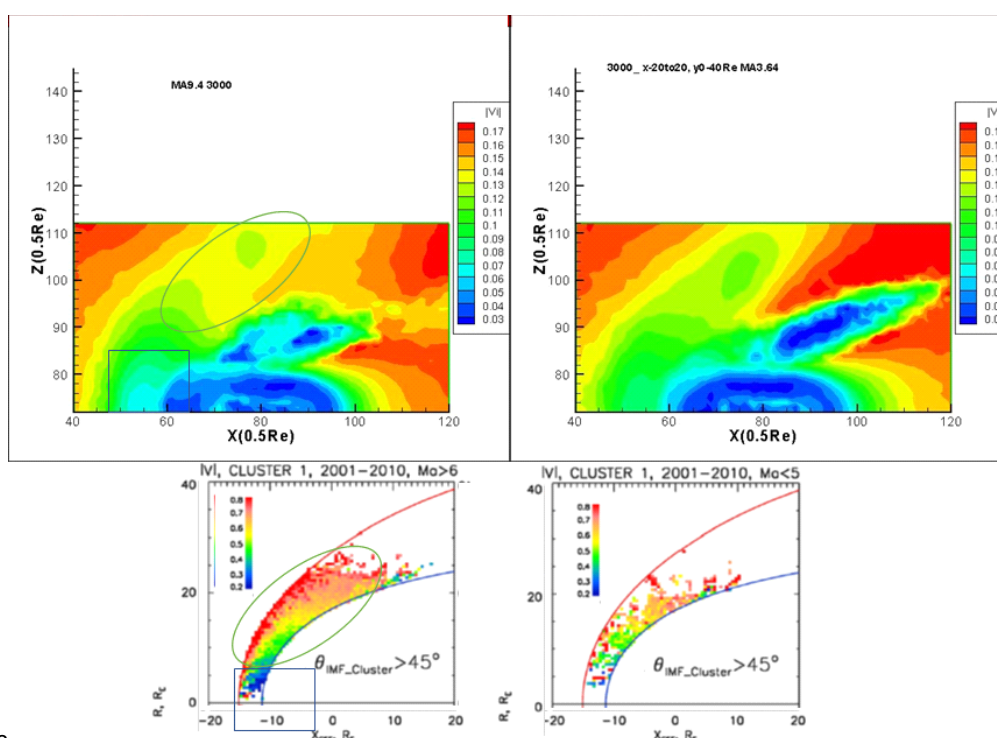
235Fig.9 current densities in the YZ plane and the results from the MHD simulation. a, b) are
 236the results from 3D PIC simulation for MA=9.4 and 3.64 respectively. C, d) are the
 237results from 3D MHD simulation (Lavraud et al 2013) for MA=9.4, 3.64 respectively.

238



239The MA=9.4 case has a higher current density (slightly bigger color scale), and both PIC
 240and MHD findings have the same structures. We do not see the current sheet bending for
 241the MA=9.4 due to the resolution of the simulation.

242



243

244Fig.10 Abstract value of ion velocity in the meridian plan. a, b) the results from 3D PIC
 245simulation for MA=9.4, 3.64 respectively. c, d) the observational data from CLUSTER
 246satellite (Lavraud et al 2013) for MA > 6, MA < 5 respectively.

247

2483-Summary and conclusion

249The effects of Alfvén Mach number on the general shape and size of the magnetosphere
 250on both meridian and equatorial planes were the focus of this paper. Furthermore, we
 251looked into the effects of various Alfvén Mach numbers on the cusp area. We explored



252 distinct MA impacts on the emergence of Kelvin-Helmholtz instability layers around the
253 Earth in the equatorial plane. During the higher scenario of $MA = 5$, we noticed a
254 narrower distance between two KHI layers, larger particle current densities, and more
255 turbulent currents centered near the Earth. In this paper, we have reported the results for
256 electron and ion behavior (currents and densities) under various Alfvén Mach numbers.
257 For the northward IMF example, we found that a greater Alfvén Mach number has a
258 significant impact on the structure and dynamics of the Earth's magnetosphere. We
259 compared the results from our 3D PIC simulation with the results from the MHD results
260 for magnetospheric dynamics at various Alfvén Mach numbers. Our findings indicated
261 good agreement with the MHD community for the compared cases. (This sentence needs
262 to be rephrased): This could be due to the cusp's which is shifted sunward morphology at
263 higher Alfvén Mach numbers. This confirms our prior findings (Esmaeili & Kalaei
264 2017), that we can only be detected double or triple cusp in a few rare circumstances.
265 This is consistent with the observation of a double/triple cusp during various satellite
266 missions. Due to the varied magnetospheric conditions, certain satellite missions do not
267 report double cusp. The double cusp region study will be worth exploring using the 3D
268 PIC global simulation.

269

270 References

- 271 Buneman, O., Neubert, T., Nishikawa, K.I.: Solar wind-magnetosphere interaction as
272 simulated by a 3-D EM particle code. *IEEE Trans. Plasma Sci.* 20(6), 810–816 (1992)
- 273 Buneman, O.: TRISTAN: the 3-D, EM particle code. In: Matsumoto, e.b.H., Omura, Y.
274 (eds.) *Computer Space Plasma Physics, Simulation Techniques and Software*, pp. 67–84.
275 Terra Scientific, Tokyo (1993)



- 276Cai, D., Esmaeili, A., Lembège, B., Nishikawa, K.-I.: Cusp dynamics under northward
277IMF using three-dimensional global particle-in-cell simulations. *J. Geophys. Res. Space*
278Phys. 120, 8368–8386 (2015). doi:10.1002/2015JA021230
- 279Esmaeili, A., Kalaei, M.J.: Double-cusp simulation during northward IMF using 3D PIC
280global code Astrophys. Space Sci. 362:125,(2017). DOI 10.1007/s10509-017-3098-8
- 281Esmaeili A, Kalaei MJ, Ikram M.: Numerical study of penetration and distribution of
282charged particles in the magnetosphere during southward IMF case. *Contributions to*
283*Plasma Physics*. e202000164 (2020). <https://doi.org/10.1002/ctpp.202000164>
- 284Fairfield, D. H., Average and unusual locations of the Earth's magnetopause and bows
285hock, *J. Geophys. Res.*, 76, 6700, (1971).
- 286Farris, M. H. & Russell, C. T. Determining the standoff distance of the bow shock: Mach
287number dependence and use of models. *J. Geophys. Res.* 99, 17681–17689 (1994).
- 288Farrugia, C. J., Erkaev, N. V., Biernat, H. K. and Burlaga, L. F., "Anomalous
289magnetosheath properties during Earth passage of an interplanetary magnetic cloud",
290JOURNAL OF GEOPHYSICAL RESEARCH, VOL. 100, NO. A10, PAGES 19,245-
29119,257, (1995)
- 292Lavraud, B. & Borovsky, J. E. Altered solar wind-magnetosphere interaction at low Mach
293numbers: coronal mass ejections. *J. Geophys. Res.* 113, A00B08 (2008).
- 294Lugaz, N., Farrugia, C.J., Huang, C.-L., Winslow, R. M., Spence, H. E. & Schwadron, N.
295A., "Earth's magnetosphere and outer radiation belt under sub-Alfvénic solar
296wind", *NATURE COMMUNICATIONS*, 7:13001(2016). DOI: 10.1038/ncomms13001
- 297Matsumoto, Y., and K. Seki, The secondary instability initiated by the three-dimensional
298nonlinear evolution of the Kelvin-Helmholtz instability, *J. Geophys. Res.*, 112,
299A06223(2007), doi:10.1029/2006JA012114
- 300Merkin, V. G., J. G. Lyon, and S. G. Claudepierre, Kelvin-Helmholtz instability of the
301magnetospheric boundary in a three-dimensional global MHD simulation during
302northward IMF conditions, *J. Geophys. Res. Space Physics*, 118, 5478–5496(2013),
303doi:10.1002/jgra.50520.
- 304Ravi Samtaney, Suppression of the Richtmyer-Meshkov instability in the presence of a
305magnetic field, *Physics of Fluids* 15, L53 (2003); <https://doi.org/10.1063/1.1591188>
- 306Shue, J.-H., Song, P., Russell, C. T., Steinberg, J. T., Chao, J. K., Zastenker, G.,
307Vaisberg, O. L., Kokubun, S., Singer, H. J., Detman, T. R., Kawano, H.: Magnetopause
308location under extreme solar wind conditions, *J. Geophys. Res.* 103, 17691–17700
309(1998).
- 310
- 311